Spectral priors improve near-infrared diffuse tomography more than spatial priors

Ben Brooksby, Subhadra Srinivasan, Shudong Jiang, Hamid Dehghani, Brian W. Pogue, and Keith D. Paulsen

Thayer School of Engineering, Dartmouth College, 8000 Cummings Hall, Hanover, New Hampshire 03755

John Weaver, Christine Kogel, and Steven P. Poplack

Department of Diagnostic Radiology, Dartmouth Hitchcock Medical Center, Lebanon, New Hampshire 03756

Received January 18, 2005

We compare the benefits of spatial and spectral priors in near-infrared diffuse tomography image reconstruction. Although previous studies that incorporated anatomical spatial priors have shown improvement in algorithm convergence and resolution, our results indicate that functional parameter quantification by this approach can be suboptimal. The incorporation of *a priori* spectral information significantly improves the accuracy observed in recovered images. Specifically, phantom results show that the maximum total hemoglobin concentration ($[Hb_T]$) in a region of heterogeneity reached 91% of the true value compared to 63% using spatial priors. The combination of both priors produced results accurate to 98% of the true $[Hb_T]$. When both spatial and spectral priors were applied in a healthy volunteer, glandular tissue showed a higher $[Hb_T]$, water fraction, and scattering power compared to adipose tissue. © 2005 Optical Society of America

OCIS codes: 110.3080, 110.6960, 170.3010, 170.3880.

In near-infrared (NIR) tomography, measurements of light remitted and transmitted through tissue, along with suitable mathematical models of light propagation, are used to obtain images of tissue constituents—total hemoglobin concentration ($[Hb_T]$), oxygen saturation (S_tO_2), water, and scatter. Qualitative, moderate-resolution images may be used to diagnose tumors based on their metabolic and functional status, but improvements in quantitative accuracy and resolution are still needed. Simulation studies and some phantom experiments have shown that anatomical information from other modalities such as magnetic resonance imaging (MRI), ultrasound, or x-ray tomosynthesis, when used in reconstruction procedures, can improve the stability of the estimation process and speed convergence to higher-resolution images.[1,2] However, priors corrupted by systematic errors and noise may bias property estimates. Brooksby *et al.*[3] encoded MRI priors into a regularization scheme, thereby relaxing the requirement that spatial constraints be error free. Phantom data at a single wavelength were used to show that quantitative accuracy and spatial resolution of optical property images could be improved without increasing the vulnerability to systematic errors. The net effect of such anatomical priors on quantitative spectroscopic accuracy is less clear.

Another type of prior incorporates the known spectral behavior of tissue chromophores and Mie scattering theory as constraints. This type of reconstruction uses multiwavelength measurements simultaneously to compute images of constituent parameters without intermediate recovery of optical properties. Corlu *et al.*[4] and Li *et al.*[5] applied the technique to continuous-wave data and showed images with improved parameter independence in simulations. Srinivasan *et al.*[6] extended the approach to the frequency domain and showed experimental evidence of improved quantification. In this Letter, we compare this latter approach of spectral priors to spatial priors when applied to experimental and clinical data. Results show that (i) spatial priors improve image resolution but can underestimate the $[Hb_T]$ of a heterogeneity, (ii) spectral priors generate superior quantification of all estimated NIR parameters, and (iii) the use of the two together produces images that are quantitatively accurate and spatially superior.

Having obtained measurements at the periphery of the phantom or breast, image reconstruction is carried out by repeated solution of the diffusion equation using the finite-element method to estimate optical properties.[7] A Newton–Raphson method is used to minimize the least-squares functional $\chi^2=\Sigma_{j=1}^{M}(\phi_j^m-\phi_j^c)^2$ for M measurements, where ϕ_j^m and ϕ_j^c are the measured and calculated fluence at the boundary, respectively. The optical property update, $\partial\mu$, is governed by the matrix equation $(\mathcal{J}^T\mathcal{J}+\alpha I)\,\partial\mu=\mathcal{J}^T\partial\phi$, where $\partial\phi=(\phi^m-\phi^c)$ and $\mathcal{J}=[\mathcal{J}_{\mu_a},\mathcal{J}_{\kappa}]$ is the Jacobian containing the derivatives of ϕ^c with respect to the optical properties $\mu=(\mu_a,\kappa)$. Here, μ_a is the absorption coefficient, $\kappa=1/[3(\mu_a+\mu_s')]$ is the diffusion coefficient, and μ_s' is the reduced scattering coefficient. α, which is initially set to ten times the maximum value of $\mathcal{J}^T\mathcal{J}$ and reduced with each iteration, controls the regularization or smoothness applied. The linear system $\mu_a=[\varepsilon]c$ is then solved for the concentrations c of oxyhemoglobin, deoxyhemoglobin, and water, where ε is the molar absorption spectra of these chromophores. The Mie theory approximation, $\mu_s'=A\lambda^{-b}$, is used to derive images of scatter amplitude A and scatter power b, where λ is the wavelength in micrometers.

Incorporating spectral relationships into the reconstruction directly, the least-squares functional includes measurements at all (n) wave-

0146-9592/05/151968-3/$15.00

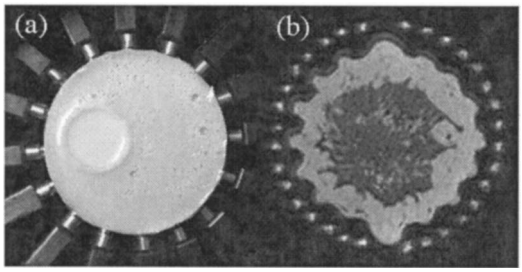

Fig. 1. (a) Cylindrical breast phantom inside our NIR system. (b) Anatomically coronal MRI of a healthy breast imaged with our simultaneous NIR–MRI system. Two tissue types are visible: fibroglandular (dark gray) and adipose tissue (light gray).

lengths. The Newton method produces the relationship $\partial\phi_\lambda = \mathcal{J}_{c,\lambda}\mathrm{d}c + \mathcal{J}_{A,\lambda}\mathrm{d}A + \mathcal{J}_{b,\lambda}\mathrm{d}b$, where $\mathcal{J}_{c,\lambda}$, $\mathcal{J}_{A,\lambda}$, and $\mathcal{J}_{b,\lambda}$ represent the Jacobians for each of the chromophore and scattering parameters. With $(\tilde{\mathcal{J}}^T\tilde{\mathcal{J}} + \alpha I)\,\partial c = \tilde{\mathcal{J}}^T\partial\phi$, where $\partial\phi = (\phi^{m,\lambda} - \phi^{c,\lambda})_{\lambda=1:n}$ and $\tilde{\mathcal{J}} = [\mathcal{J}_{c,\lambda}, \mathcal{J}_{A,\lambda}, \mathcal{J}_{b,\lambda}]_{\lambda=1:n}$, the update occurs in terms of c, A, and b, directly.[6]

To introduce spatial constraints, the minimization functional is modified to include a penalty term, becoming $\hat{\chi}^2 = \Sigma_{j=1}^{Mn}(\phi_j^m - \phi_j^c)^2 + \beta\Sigma_{j=1}^{NN}L(\mu_j - \mu_{o,j})^2$, where β is the regularizing factor for the spatial prior, NN is the number of unknowns sought, and L is a matrix generated from MRI-derived spatial data acting on the solution μ. The L constructed here applies a second-derivative filter to all locations (nodes) in a particular tissue type (glandular or fatty), but not across internal boundaries, preserving sharp edges.[3] Setting the first derivatives of $\hat{\chi}^2$ with respect to each of the parameters sought equal to zero, the final matrix equation that is solved iteratively becomes $(\tilde{\mathcal{J}}^T\tilde{\mathcal{J}} + \beta L^T L)\,\partial c = \tilde{\mathcal{J}}^T\partial\phi$. The effects of L and β on reconstructed μ_a and μ_s' images were characterized in simulation and phantom studies, accounting for measurement noise and error in the spatial prior.[3] Results indicate that setting β to ten times the maximum value of $\tilde{\mathcal{J}}^T\tilde{\mathcal{J}}$ optimizes image quality and accuracy regardless of the level of geometric complexity present.

A phantom and a clinical case study are presented here to evaluate these spectral and spatial constraints. Figure 1(a) shows a gelatin phantom placed inside our NIR imaging array. The gelatin properties include $[\mathrm{Hb_T}] = 23\ \mu\mathrm{M}$, $\mathrm{S_tO_2} = 72\%$, $\mathrm{H_2O} = 57\%$, $A = 0.65$, and $b = 1.35$. Near the edge is a 25 mm cylindrical cavity that was filled with Intralipid solutions with varying $[\mathrm{Hb_T}]$. Figure 1(b) shows an anatomically coronal T1-weighted MRI of an asymptomatic volunteer imaged with our combined NIR–MRI system.[8] NIR measurements were acquired at six wavelengths (661, 761, 785, 808, 829, and 849 nm) for both the phantom and the clinical case.

Figure 2 (top row) shows the true properties of the phantom with an inclusion, along with images reconstructed with four algorithms. The first uses no priors—absorption and reduced scattering coefficients are reconstructed at each wavelength, then spectrally decomposed to produce images of the $[\mathrm{Hb_T}]$, $\mathrm{S_tO_2}$, the water fraction, A, and b (second row). The second, third, and fourth algorithms incorporate spatial, spectral, and both spatial and spectral priors, respectively, and their images appear in the third, fourth, and fifth rows of Fig. 2. Spatial priors are derived from Fig. 1. The conventional method (no priors) yields images with considerable artifacts. Spatial priors remove these, so that the inclusion is clearly visible and matches the expected size and shape. However, the $[\mathrm{Hb_T}]$ contrast is significantly underestimated. The recovered mean in the region of the anomaly reaches only 57% of the true value (the maximum reaches 63% of the true value). Spectral priors show substantial improvement in the quantification with the mean $[\mathrm{Hb_T}]$ at 78% of the true value (maximum at 91%). Finally, the application of both constraints results in images with further reduction in artifacts close to the boundary, and the mean $[\mathrm{Hb_T}]$ reaches 88% of the expected value (maximum at 98%).

The experiment was carried further using four different blood concentrations in Intralipid solution as inclusions ($22–43\ \mu\mathrm{M}\ [\mathrm{Hb_T}], \mathrm{S_tO_2} = 100\%$, water $= 100\%$, $A = 0.65, b = 1.35$). Figure 3 shows the mean property values recovered in the region of interest for each change in $[\mathrm{Hb_T}]$ by applying the four methods of reconstruction. As suggested in Fig. 2, although the standard deviation in the region of interest is reduced using spatial constraints (leading to smoother images), the values are underestimated and may even be degraded relative to the reconstruction without any priors. The spectrally constrained technique improves $[\mathrm{Hb_T}]$ accuracy, and including both priors gives the best results: accurate quantification along with reduced standard deviation.

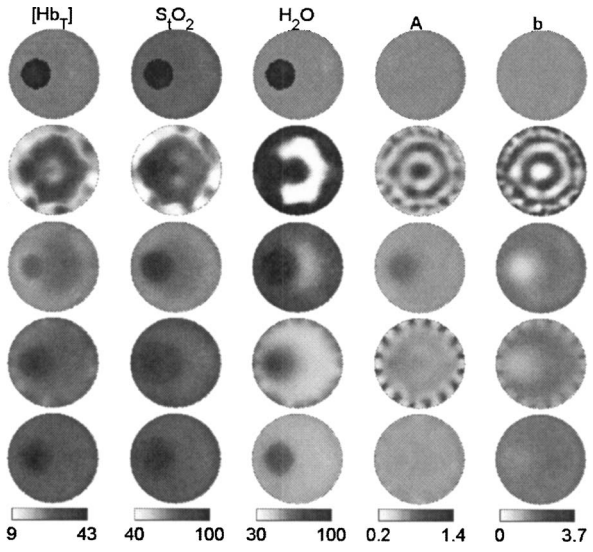

Fig. 2. Images of total hemoglobin concentration (μM), oxygen saturation (%), water (%), scattering amplitude, and scattering power for the phantom. The top row shows the true values, the second shows the reconstruction that uses no priors, the third uses spatial constraints, the fourth uses spectral constraints, and the bottom uses both spectral and spatial priors.

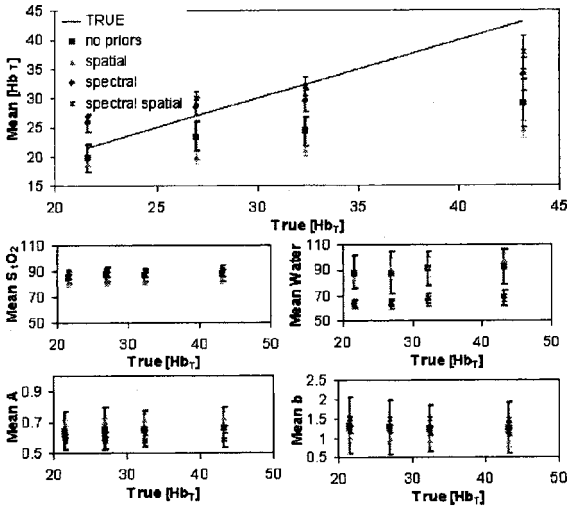

Fig. 3. Mean reconstructed values of $[Hb_T](\mu M)$, S_tO_2 (%), water (%), A, and b, in the region of the inclusion using four algorithms. When the blood concentration is high, the best results are achieved by combining spectral and spatial priors. As expected, S_tO_2, water, A, and b within the cavity remain constant.

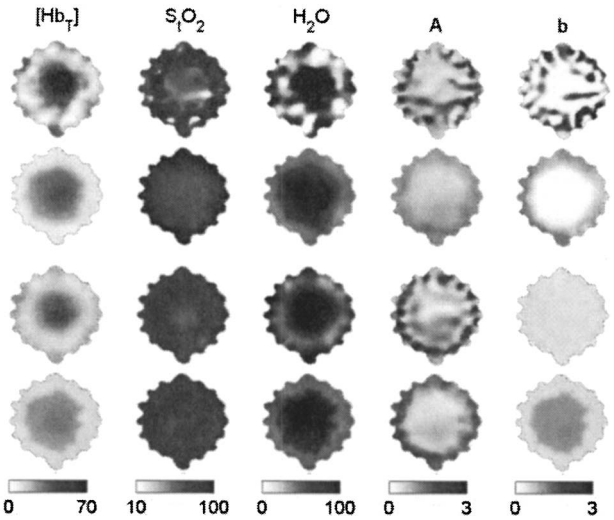

Fig. 4. Breast property images for a healthy volunteer. First (top), only the outer boundary of the tissue and optical fiber positions are specified. Second, the algorithm used spatial constraints derived from the MRI [Fig. 1(b)] related to the internal distribution of adipose and glandular tissue. Third, spectral constraints were applied and chromophore concentrations and scattering parameters were reconstructed directly. Fourth (bottom), spatial and spectral constraints were combined.

Our combined NIR–MRI imaging system was used in a case study to estimate the properties of normal breast tissue. A finite-element method mesh generated from the MRI in Fig. 1(b) was used in the reconstruction. Using the MRI gray scale, each mesh point was associated with glandular or adipose tissue. Figure 4 shows the tissue properties estimated by the four procedures used in the phantom study. The images obtained using an unconstrained reconstruction exhibit boundary artifacts. The spatial priors make these images smoother but preserve the trends in chromophore and scattering quantification. Previous studies suggest that glandular tissue has a higher number density of scatterers and may therefore have a greater scatter power than fat. Hence, the results from the spatially constrained reconstruction, although appearing smoother, may be misleading. The scatter power image obtained by the spectrally constrained method (row 3) is more quantitatively acceptable. Including the spatial priors within this spectral method (row 4) produces the most intuitively appealing image for this parameter by also showing the layered structure of the breast. We observed elevated $[Hb_T]$ (25:13 μM), water (91:49%), and scattering power (1.0:0.5) in glandular relative to adipose tissue by using the combined priors, which matches the higher degree of vascularization expected.

Intes *et al.*[9] and Li[10] showed in simulation studies that the combination of spatial and spectral priors improves the accuracy and quality of NIR images, but this Letter provides the first analysis, to our knowledge, of their individual benefits with experimental measurements. With our implementation, anatomical information improves image quality by reducing artifacts but does not significantly improve functional parameter quantification. The spectral prior obtained by including the intrinsic behavior of tissue chromophores and scattering plays a more important role in preserving quantitative functional parameter estimates. A synergy between these two priors yields the most accurate characterization of breast tissue properties currently available.

This work was funded by National Institutes of Health research grants RO1CA69544, PO1CA80139, and U54CA105480 and by U.S. Department of Defense grant DAMD17-03-1-0405. B. Brooksby's e-mail address is Ben.A.Brooksby.Th05@Alum.Dartmouth.org; B. Pogue's is Brian.Pogue@Dartmouth.edu.

References

1. M. Schweiger and S. R. Arridge, Phys. Med. Biol. **44**, 2703 (1999).
2. V. Ntziachristos, A. G. Yodh, M. D. Schnall, and B. Chance, Neoplasia **4**, 347 (2002).
3. B. Brooksby, S. Jiang, H. Dehghani, B. W. Pogue, K. D. Paulsen, J. Weaver, C. Kogel, and S. P. Poplack, "Combining near infrared tomography and magnetic resonance imaging to study *in vivo* breast tissue: implementation of a Laplacian-type regularization to incorporate MR structure," J. Biomed. Opt. (to be published).
4. A. Corlu, T. Durduran, R. Choe, M. Schweiger, E. M. Hillman, S. R. Arridge, and A. G. Yodh, Opt. Lett. **28**, 2339 (2003).
5. A. Li, Q. Zhang, J. P. Culver, E. L. Miller, and D. A. Boas, Opt. Lett. **29**, 256 (2004).
6. S. Srinivasan, B. W. Pogue, S. Jiang, H. Dehghani, and K. D. Paulsen, Appl. Opt. **44**, 1858 (2005).
7. K. D. Paulsen and H. Jiang, Appl. Opt. **35**, 3447 (1996).
8. B. A. Brooksby, S. Jiang, H. Dehghani, C. Kogel, M. Doyley, J. B. Weaver, S. P. Poplack, B. W. Pogue, and K. D. Paulsen, Rev. Sci. Instrum. **75**, 5262 (2004).
9. X. Intes, C. Maloux, M. Guven, T. Yazici, and B. Chance, Phys. Med. Biol. **49**, N155 (2004).
10. A. Li, "Diffuse optical tomography with multiple priors," Ph.D. dissertation (Tufts University, 2005).